ScienceDirect
ELSEVIER
Electrochimica Acta 52 (2007) 5815–5823
Acta
www.elsevier.com/locate/electacta

Characterization of the reaction environment in a filter-press redox flow reactor

C. Ponce-de-León [a], G.W. Reade [b,1], I. Whyte [b,2], S.E. Male [b,3], F.C. Walsh [a,*]

[a] *Electrochemical Engineering Group, School of Engineering Sciences, University of Southampton, Highfield, Southampton SO17 1BJ, UK*
[b] *Regenesys Technologies Limited, OTEF, Aberthaw Power Station, Barry, Vale of Glamorgan CF62 4QT, UK*

Received 26 October 2006; received in revised form 23 February 2007; accepted 27 February 2007
Available online 4 March 2007

Abstract

The characteristics of a divided, industrial scale electrochemical reactor with five bipolar electrodes (each having a projected area of 0.72 m^2) were examined in terms of mass transport, pressure drop and flow dispersion. Global mass transport data were obtained by monitoring the (first order) concentration decay of dissolved bromine (which was generated *in situ* by constant current electrolysis of a 1 mol dm^{-3} $NaBr_{(aq)}$). The global mass transport properties have been compared with those reported in the literature for other electrochemical reactors. The pressure drop over the reactor was calculated as a function of the mean electrolyte flow velocity and flow dispersion experiments showed the existence of slow and fast phases, two-phase flow being observed at lower velocities.

Keywords: Activated carbon electrode; Bromide ion; Bromine; Energy storage; Filter-press cells; Flow dispersion; Mass transport; Pressure drop; Redox flow battery; Reaction environment; Tribromide ion

1. Introduction

Electrochemical reactor design [1] involves careful consideration of the reaction environment to provide uniform current and potential distribution as well as heat and flow dispersion [2,3]. The filter-press cell type electrochemical reactor with parallel-plate electrode geometry is the most popular choice for many laboratory and large-scale industrial applications [4]. Reasonable rates of mass transport and good flow dispersion can be realised with this geometry, which also facilitates modular expansion and predictable scale-up [5,6]. The parallel plate cell configuration is widely used in many large-scale electrochemical processes, such as the production of chlorine and caustic soda, adiponitrile and pharmaceuticals [3,7,8].

Other electrolytic cell studies involving bipolar electrodes in a parallel cell configuration include: organic electrosynthesis [9,10], reduction of NO by CO or C_3H_6 in the presence of O_2, from a lean-burn or diesel engine [11], mass transport effects on current distribution in bipolar electrodes [12], water treatment [13–15], fluorination of organic compounds [16], production of ethane oxide [17], oxidation of cyanides [18], rechargeable batteries [19], fuel cells [20–22], solid oxide fuel cells [23,24], super-capacitors [25] and metal electrodeposition [26].

Bipolar filter-press cells of the type investigated in this paper have been developed as redox flow batteries for energy storage and load levelling purposes [27–29]. The redox flow batteries consist of two electrolytes recycled through bipolar cells from large reservoirs; chemical and electrical energy can be interchanged by reversible electrochemical reactions that take place on the electrodes when the electrolytes are charged or discharged [30–34]. The electrolytes are charged when electrical current is applied between the two electrodes and they are pumped through the reactor, if the electrical energy is needed the reactions are reversed and the energy can be withdrawn from the cell. A number of electrochemical redox couples have been used to store electrical energy, the most common are: V(II)/V(III); V(IV)/V(V), Fe(II)/Fe(III); Cr(III)/Cr(VI); Zn(0)/Zn(II); polysulfide/sulfide; Br_3^-/Br^-. The electrochemical reactor described in this paper was constructed after a series of laboratory bench-scale bipolar electrolysers (area < 0.015 m^2)

* Corresponding author. Tel.: +44 2380 598752.
E-mail address: f.c.walsh@soton.ac.uk (F.C. Walsh).
[1] Present address: Rolls Royce plc, PO Box 31, Derby DE24 8BJ, UK.
[2] Present address: Potential Reactions Limited, Milton Keynes MK8 8LR, UK.
[3] Present address: Department of Materials Science & Metallurgy, University of Cambridge, Cambridge CB2 3QZ, UK.

0013-4686/$ – see front matter © 2007 Elsevier Ltd. All rights reserved.
doi:10.1016/j.electacta.2007.02.080

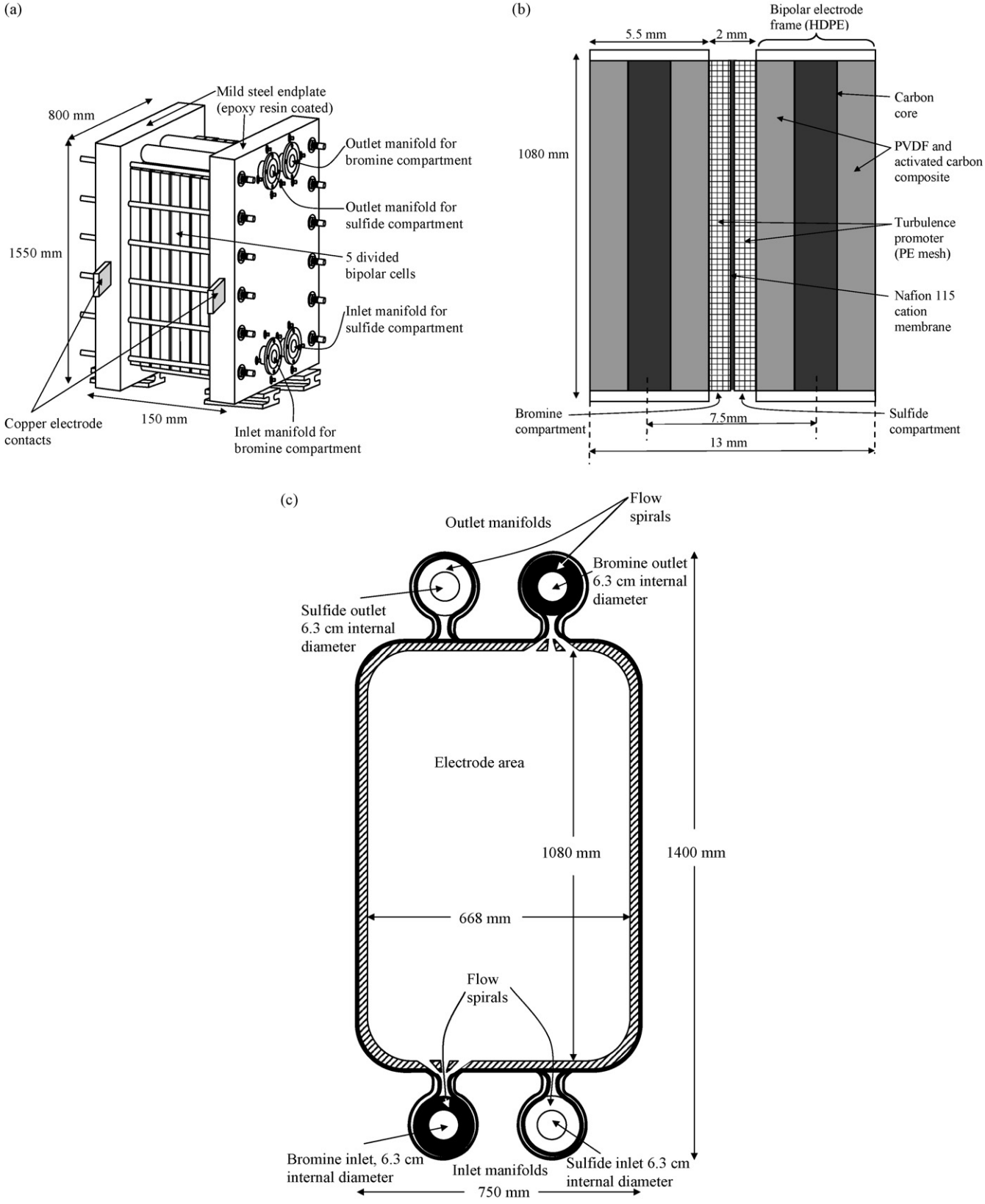

Fig. 1. (a) Lateral view of the reactor showing the inlet and outlet manifolds and the location of the current collectors. Not to scale. (b) Details of a bipolar cell showing the main components. Not to scale. The dimensions are nominal. (c) Electrode configuration showing the location of the spirals and the projected electrode area.

were studied [27]. The reactor was constructed after careful analysis of previous data on smaller laboratory and industrial pilot scales. A stack of 200 bipolar cells in this type of reactor was tested with the Na_2S/NaBr system, as one of the largest examples of electrochemical energy storage [35]. The objective of this paper is to characterize a five cell bipolar reactor, in terms of global mass transport, pressure drop and flow dispersion.

2. Experimental details

2.1. Electrochemical reactor and flow circuit

The electrochemical reactor is shown in Fig. 1(a) and consists of a bipolar stack of five cells. Prior to use, the reactor passed a 0.7 bar, 3-day hydraulic (water) test at room temperature. The reactor consists of two mild steel endplates which are epoxy resin coated each 80 cm × 155 cm × 4 cm, compressing a stack of five bipolar cells as shown in Fig. 1(a). Each bipolar cell consists of two electrodes with a projected area of 0.72 m^2 (66.8 cm × 108.0 cm) with an inter-electrode gap of 0.2 cm divided by a Nafion® 115 cation exchange membrane forming two compartments as shown in Fig. 1(b). The cross sectional area of each compartment, perpendicular to the flow direction, is 6.5 cm^2 and each compartment contained a high-density polyolefin (HDPE, Netlon™) turbulence promoter having a volumetric porosity of approximately 73%, a 45° cross pattern, a strand thickness of 0.45 mm and an overall thickness of 0.90 ± 0.05 mm.

Each bipolar electrode consisted of carbon composite core sandwiched between activate carbon/polymer layers by a laminar process. The carbon composite was manufactured from graphite particles and high density polyethylene (HDPE). The weight ratio of carbon to polymer was approximately 50:50. A mixture of polyvinyldene fluoride (PVDF) and activated carbon was compressed onto each side of the core using temperatures in the range of 150–250 °C at pressures between 0.5 and 5 MPa. The resulting laminate had an outer electrode layer of approximately 2 mm thickness. The moulded electrode was laser welded into a HDPE polymer frame. The activated carbon used in the mixture had a surface area in the range of 800–1500 $m^2\ g^{-1}$; the structure formed by the activated carbon and the polymeric material contained approximately 20% of polymeric binder. Further details of the electrode construction can be found in the literature [36]. Fig. 1(c) shows an example of a single, injection moulded frame. The electrolyte inlets and outlets consisted of 6.3 cm (2.5 in.) internal diameter chambers formed by the manifolds of the electrode frames; the manifolds contained a spiral where the electrolyte circulated before contacting the electrodes in each compartment. The spirals were designed to reduce the bypass current between the conductive pathways of the electrolyte by creating a labyrinth pathway for the electrolyte between the electrolyte circuit and the electrode compartments. Details of the geometry and incorporation of the spirals into the electrode frame can be found elsewhere [37]. The hydraulic circuit in Fig. 2 shows the position of pressure, temperature, conductivity sensors and Luggin capillary ports. Each electrode compartment was connected to a 2.54 cm (1 in.) pipeline via 6.3 cm (2.5 in.)

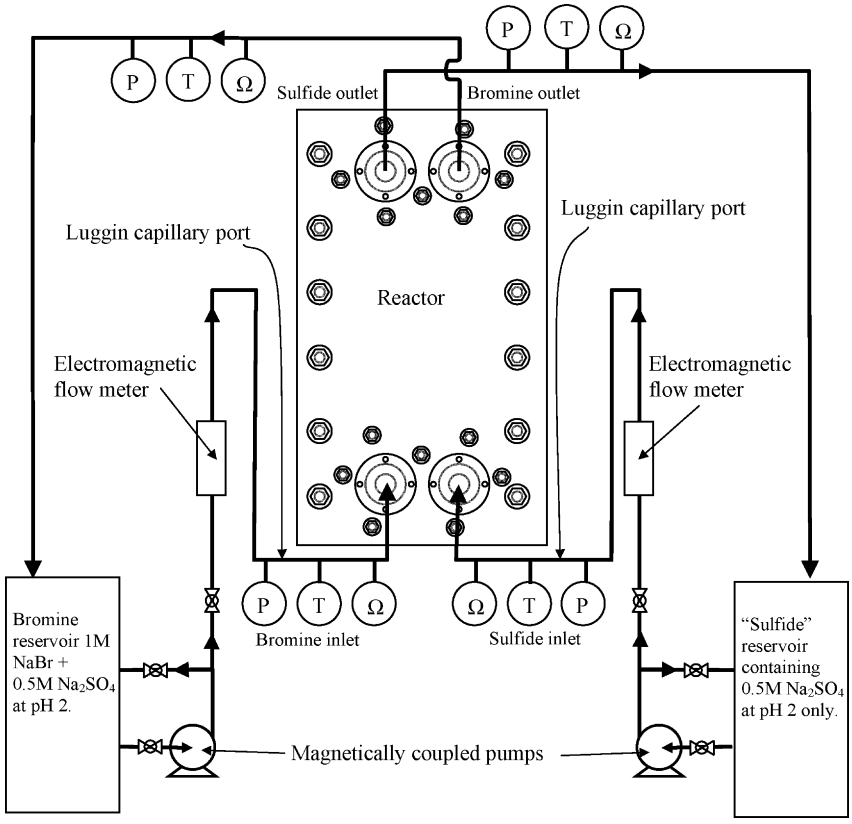

Fig. 2. Schematic view of the reactor and the electrolyte flow circuit.

Table 1
Essential reactor details

Electrode material	Polyvinylidene-difluoride (PVdF) and activated carbon composite laminated on HDPE/carbon core
Number of bromine compartments in the cell stack (reactor)	5
Membrane material	Nafion 115 cation exchange (ca. 125 μm dry film thickness)
Interelectrode gap	1.8–2.1 mm
Electrode to membrane gap, S	0.9–1.05 mm
Length of electrode, L	108 cm
Breadth of electrode, B	66.8 cm
Geometrical area of the electrode, A	7200 cm^2
Equivalent diameter of flow channel, d_e	0.19 cm
Channel volume, $V = LBS$	700 cm^3
Volumetric flow rate through each compartment module, Q	0–24,000 $cm^3\ min^{-1}$, 0–1.44 $m^3\ h^{-1}$
Internal diameter of the inlet and outlet manifolds	6.3 cm
Mean linear flow velocity of the electrolyte, v	0–12.5 $cm\ s^{-1}$
Mean residence time in the reactor compartment, τ_R	8.7–210 s
Mean residence time in the tank, τ_T	5.2–125 s

flange both at the inlets and outlets of the electrolyte. Small, 0.2 cm internal diameter tubes were inserted at the pipeline at the inlet of the electrolyte in both compartments before the spirals to serve as Luggin capillaries in order to monitor the electrode potential. Table 1 shows a summary of the reactor details.

The reactor was designed to operate with the Na_2S/NaBr redox system [35]. The electrolyte circuit designed for the Na_2S solution was assembled with PVC-U fittings whereas the circuit designed for the NaBr solution was constructed with PVdF pipeline. Due to the spatial arrangement of the two compartments and the position of the two spirals in the inlet manifolds, aiming to reduce the bypass current, the compartment designed to contain the polysulfide solution was slightly larger than the compartment designed for the NaBr solution. The results presented in this work, refer to the compartment designed to contain the NaBr system only. In this work, the "polysulfide" compartment designed to contain the Na_2S solution was used with Na_2SO_4 1 mol dm^{-3} solution adjusted to pH 2 with H_2SO_4 for the purpose of cell characterisation, Na_2S was not employed. The physical and transport properties of the NaBr electrolyte are shown in Table 2.

Table 2
Characteristic properties of the electrolyte

Electrolyte composition	1 mol dm^{-3} of NaBr in 0.5 mol dm^{-3} Na_2SO_4 at pH 2	Reference
Temperature	298 ± 3 K	–
Fluid density, ρ	1.076 g cm^{-3}	[42]
Dynamic viscosity, η	0.0106 g $cm^{-1}\ s^{-1}$	[42]
Kinematic viscosity, $\nu = \eta/\rho$	0.0098 $cm^2\ s^{-1}$	–
Diffusion coefficient of Br^-, D	1.24×10^{-5} $cm^2\ s^{-1}$	[43]
Schmidt number, $Sc = \nu/D$	926	–

Typically, experiments were carried out with 50 dm^{-3} of electrolyte in each reservoir (see Fig. 2) and the solutions were continuously recycled through the compartments of the cell in a ventilated fume hood. The flow rate of the electrolyte in each compartment was controlled by adjusting the rotation frequency of the electromagnetically coupled pumps (March–May, model TE-7MD, 0.75 kW) using a frequency controller (Telemecanique, model Altivar 08). Flow velocities were measured with electromagnetic flow meters (Endress plus Hauser model Picomag II), with 8 mm nominal diameter and measurement range 0–24 $dm^3\ min^{-1}$. The reservoirs were made of PVdF and the fluid tubing was 25 mm diameter PVC-U and/or PVdF. Experiments were carried out at 298 ± 3 K.

2.2. Mass transport measurements

Following the constant current electrolysis of 1 mol dm^{-3} NaBr in 0.5 mol dm^{-3} Na_2SO_4 at pH 2, the electrode in the bromine compartment was made cathodic to reduce the dissolved bromine. Averaged mass transport coefficients were obtained from the semilogarithmic plots of the concentration decay of dissolved bromine against time. The sulfide compartment contained Na_2SO_4 electrolyte at pH 2 only, as no Na_2S solution was used. The current was applied with a regulated dc power supply (Farnell model AP60-150). Typically, the applied current was 100 A (138.6 A m^{-2}) during 1 h after which the power supply was disconnected and the two electrical terminals of the reactor were short-circuited; this caused the reduction of bromine to bromide ion to be mass transport controlled. The concentration of bromide ion was determined potentiometrically by a combined ion selective electrode, radiometer model ISE25Br with a solid-state sensor at 298 ± 3 K. The concentration values were confirmed by titration of the residual bromine in selected samples with standardised 0.1 mol dm^{-3} $Na_2S_2O_3$. The Br^- ISE electrode was equilibrated with NaBr solutions in 0.5 mol dm^{-3} Na_2SO_4 at pH 2 at concentration close to those expected from the samples and calibrated each time a new set of samples from a different experiment was measured. The concentration decay of dissolved bromine was determined at mean linear flow velocities in the range 0.27–4.4 $cm\ s^{-1}$.

2.3. Pressure drop measurements

Pressure transducers (Sensors Technique model PS20030G) were located on the pipelines at the inlet and outlet of the electrolyte compartments. The pressure was monitored electronically via a purpose built PC data acquisition system and the pressure transducers were calibrated using a portable pressure calibrator (Druck DPI 603). The pressure drop, Δp was measured maintaining the same volumetric flow rate in both compartments of the reactor following the flow dispersion experiments and using, for convenience, the same electrolyte solution; 1% NaCl aqueous solution at room temperature (≈298 ± 3 K).

2.4. Flow dispersion measurements

At the reactor inlet, 20 mL of saturated KCl solution (≈3.5 mol dm^{-3}) was manually injected with a syringe; the

plunger area of the syringe was found small enough to allow manual injections lasting 1–2 s at the highest flow rates, while maintaining the same mean linear electrolyte velocity in both compartments. The electrolyte collected at the top of the cell was stored in a different container to the solution feed to the reactor. A conductivity probe (Russell type CDC33) was mounted in a T-piece at the exit of the electrolyte pipeline; the probe consisted of platinised platinum foil electrodes (1.39 cm^{-1} cell constant) connected to a conductivity meter (Metrohm 712). The conductivity of the electrolyte was monitored *versus* time by connecting the conductivity meter to a chart recorder until a steady state baseline reading was achieved. The pulse injection then took place and the increase in conductivity of the reactor outlet was followed with time. Studies were restricted to the region in which the conductance of aqueous KCl was directly proportional to its concentration. Dispersion experiments were carried out at a mean linear velocity in the range of 1.0–10.4 $cm\,s^{-1}$ in the bromine compartment. The experiments were conducted at room temperature (≈298 ± 3 K).

3. Results and discussion

3.1. Mass transport rates

During the electrolysis of 1 $mol\,dm^{-3}$ NaBr in 0.5 $mol\,dm^{-3}$ Na_2SO_4 at pH 2, the main electrochemical reactions are:

$$\text{bromine compartment}: \ 3Br^- - 2e^- \rightarrow Br_3^- \quad (1)$$

$$\text{hydrogen compartment}: \ 2H^+ + 2e^- \rightarrow H_{2(g)} \quad (2)$$

Although the concentration of soluble bromide ion was nominally 1 $mol\,dm^{-3}$, the typical measured values in solution were lower, of the order of 0.9 $mol\,dm^{-3}$, since some adsorption of bromide ions occurred onto the activated carbon electrodes. After the electrolysis, the concentration of bromide ions was less than 0.1 $mol\,dm^{-3}$ (≈90% conversion) while the concentration of dissolved bromine increased from 0 to ≈0.3 $mol\,dm^{-3}$. The current efficiency to produce this concentration of bromine was only 16% however, since the purpose of the experiment was to produce bromine to measure the concentration decay of dissolved bromine under mass transport conditions, the low current efficiency was not relevant. During the electrolysis, the potential of the cell stack gradually increased from 0 to 14 V while the potential of the electrode in contact with the bromine compartment increased from 0.1 to 4–10 V *versus* SCE. After one hour of electrolysis, the dc power supply was disconnected and it was observed that the open-circuit potential of the cell stack was approximately 0.2 V. After disconnecting the power supply, the terminals of the reactor were carefully short-circuited causing the reverse of reactions (1) and (2). It was assumed that some of the hydrogen gas generated during the electrolysis was stored in the pores of the activated carbon electrodes and that this hydrogen gas was oxidised when the reactor electrical terminals were short-circuited.

Following the connection of the two terminals of the cell, the potential of the cell stack gradually dropped from 0.2 to 0 V as the dissolved bromine was consumed. The potential of the bromine electrode compartment changed from +1.2 to −0.4 V *versus* SCE. These values agree with the potentials expected in a solution were the concentration of bromide ions is increasing. The potential of the other electrode were the oxidation of hydrogen gas took place, increased from −1.5 to +0.2 V *versus* SCE according to the potential expected when hydrogen gas was consumed.

Fig. 3 shows the logarithmic plot of the normalized bromine concentration decay *versus* time at selected flow rates. The concentration of bromine decreased to nearly zero in all cases and the concentration decay was faster as the mean linear velocity of the electrolyte increased. The decay was exponential with time, which can be confirmed by a plot of $\log[c_{(t)}/c_{(0)}]$ *versus* time, as shown in Fig. 3, and the decay was approximately linear over a two-decade change in dissolved bromine concentration. The concentration decay could be approximated by the 'plug flow reactor in batch recycle' model [38,39]. Assuming that the system conforms to this model, the normalised reactant concentration in the tank at time t may be described by [1,2,34]:

$$\log\left(\frac{c_{(t)}}{c_{(0)}}\right) = -2.3\frac{t}{\tau_T}\left[1 - \exp\left(-\frac{k_m A}{Q}\right)\right] \quad (3)$$

where A, k_m, t, τ_T, c and Q are the geometrical electrode area, mass transport coefficient, time, mean residence time in the tank, reactant concentration in the tank and volumetric flow rate. The log–log plot presented in Fig. 4 summarises mass transport coefficient values for the bromine compartment of the reactor calculated via the above model. The log–log plots suggest a linear correlation of the form:

$$k_m = av^b \quad (4)$$

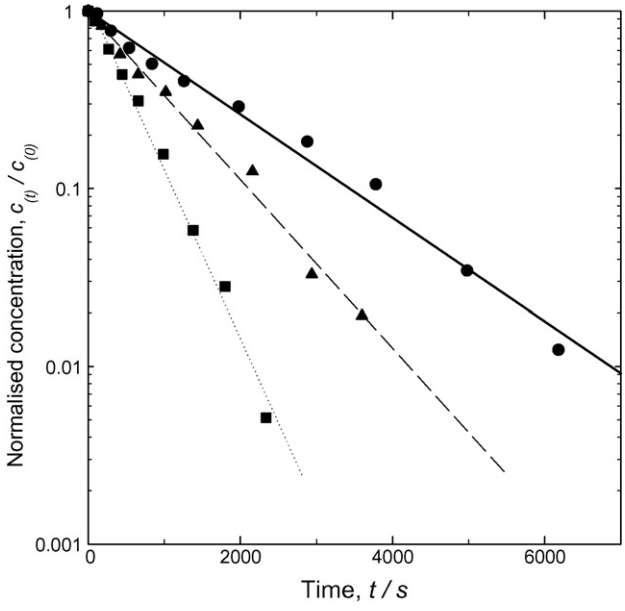

Fig. 3. Semilogarithmic plot of the normalised concentration of dissolved bromine in the bromine compartment, during the short-circuit of the reactor. Initial Br_2 concentration: 0.25–0.3 $mol\,dm^{-3}$ Na_2SO_4 in 0.5 $mol\,dm^{-3}$ at pH 2 and mean linear flow velocities; (●) 1 $cm\,s^{-1}$, (π) 2 $cm\,s^{-1}$, (■) 4 $cm\,s^{-1}$.

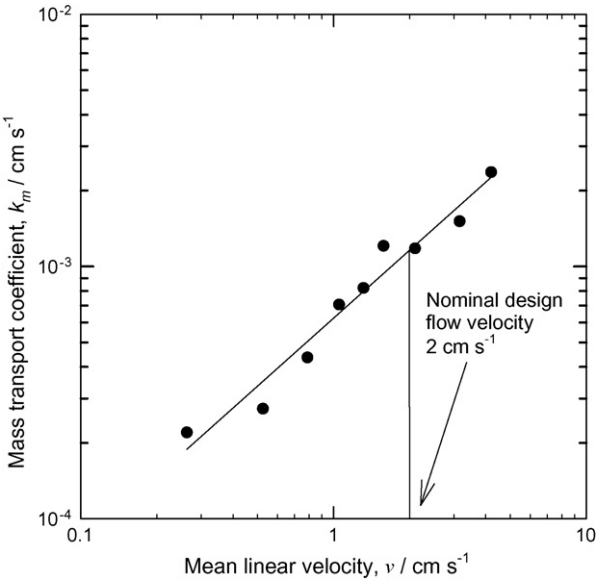

Fig. 4. log–log plot of the mass transport coefficient, k_m *vs.* the mean linear flow velocity, v for the bromine reactor compartment.

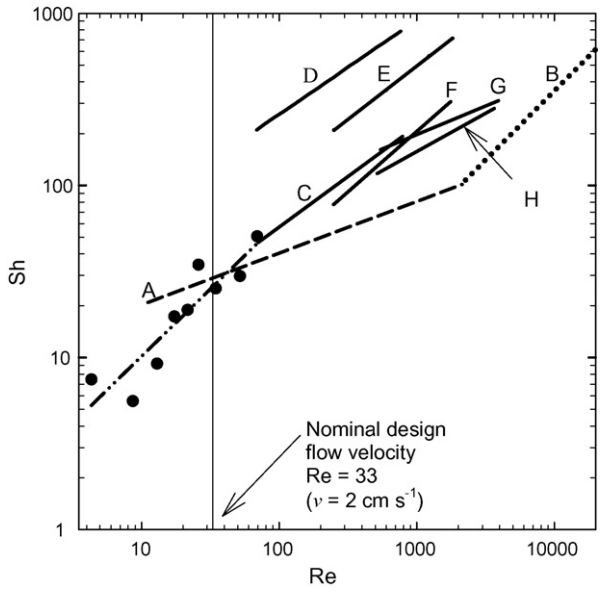

Fig. 5. (●) log–log plot of *Sh vs. Re* for the reactor compared with the theoretical values for a laminar and turbulence flow in a rectangular channel and other electrolytic cells [5,39–41]. The letters on the lines correspond to those specified in Table 3.

The value of the velocity exponent varied between 0.79 and 0.89. Mass transport properties can be compared with other electrochemical systems by casting the data into a dimensionless group correlation. Such relationship can be expressed as a function of the dimensionless numbers Sherwood, Reynolds and Schmidt in the following equation:

$$Sh = a\,Re^{b}\,Sc^{1/3} \tag{5}$$

The Sherwood and Reynolds numbers are defined as:

$$Sh = k_{\mathrm{m}}\frac{d_{\mathrm{e}}}{D} \tag{6}$$

$$Re = v\frac{d_{\mathrm{e}}}{\nu} \tag{7}$$

where D is the diffusion coefficient, v the mean linear electrolyte flow velocity, ν the kinematic viscosity and d_{e} is the hydraulic diameter, calculated from:

$$d_{\mathrm{e}} = \frac{2BS}{B+S} \tag{8}$$

B is the breadth of the electrode and S is the separation between the electrode and the membrane. The physical and transport properties of the electrolyte presented in Table 2 were used for the evaluation of Eq. (5) and the exponent on the Schmidt number was assumed to be 0.33 [1,34]. The plot of the *Sh versus Re* correlation for the bromine compartment of the reactor is shown in Fig. 5 together with the dimensionless correlation for an ideal laminar flow and other electrochemical systems reported in the literature such as the FM21-SP and the DEM cells [5,38–41]. The present reactor can realise reasonable values of the mass transport coefficients at the low linear velocities. The values of the best-fit mass transport correlations for each electrochemical system presented in Fig. 5 are shown in Table 3.

3.2. Pressure drop

The pressure drop Δp, was measured as a function of the fluid velocity across the total cell stack that includes the outlet

Table 3
Dimensionless mass transport correlations for parallel plate electrodes

Cell	Geometry and flow	Conditions	$Sh = a\,Re^{b}\,Sc^{c}$			Reference
			a	b	c	
Present	Laminar (bromine compartment)	$A = 7214$ cm^2, $20 < Re < 120$, $Sc = 926$	0.18	0.78	0.33	This work
A	Fully developed laminar in channel	$Re < 2300$, $L = 35d_{\mathrm{e}}$	2.54	0.3	0.33	[39]
B	Fully developed turbulent in channel	$Re < 2300$, $L = 12.5d_{\mathrm{e}}$	0.023	0.8	0.33	[39]
	Electrosyncell					[39]
C	Flat plate	$70 < Re < 800$	0.39	0.58	0.33	
D	Flat plate plus grid	Area = 440 cm^2, $Sc = 1572$	5.57	0.40	0.33	
E	FM21-SP flat plate + turbulence promoter	$A = 2250$ cm^2, $d_{\mathrm{e}} = 2$ cm, $65 < Re < 450$, $Sc = 1562$	1.18	0.62	0.33	[5]
F	FM21-SP flat plate only	$A = 2250$ cm^2, $d_{\mathrm{e}} = 2$ cm, $250 < Re < 1800$, $Sc = 1562$	1.04	0.70	0.33	[5]
G	DEM cell divided with turbulence promoter	$550 < Re < 4000$, $Sc = 1465$	1.91	0.32	0.33	[40]
H	DEM cell undivided with turbulence promoter	$550 < Re < 4000$, $Sc = 1465$	0.66	0.44	0.33	[40]

The Sc number was assumed to be 1000 [40]. The letters correspond to the labels in Fig. 5.

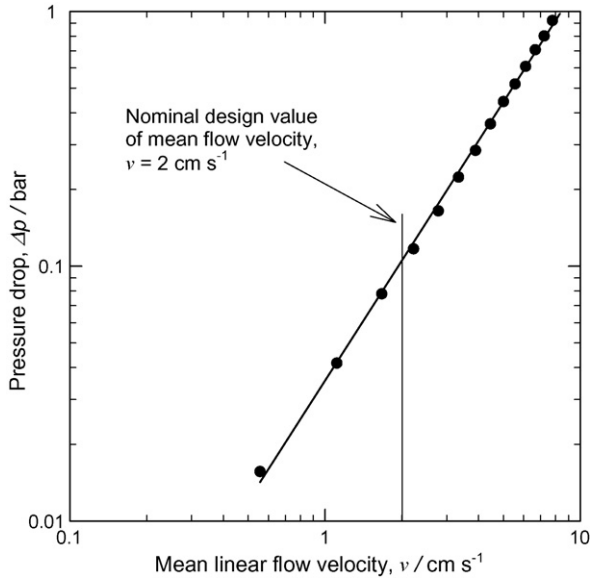

Fig. 6. log–log plot of pressure drop *vs.* mean linear flow velocity of electrolyte for the bromine compartment of the reactor.

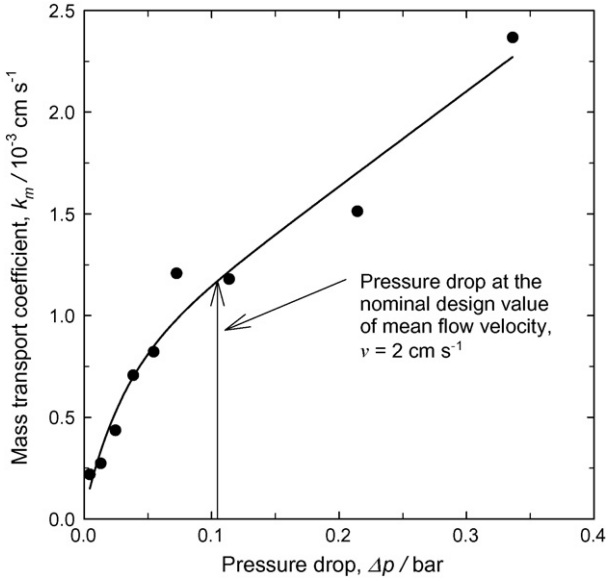

Fig. 7. Mass transport coefficient *vs.* pressure drop for the reactor. The electrolyte was 1 mol dm^{-3} NaBr in 0.5 mol dm^{-3} Na_2SO_4 at pH 2 in one compartment while Na_2SO_4 at pH 2 was used in the other compartment.

and inlet manifolds, spirals and flow channels of the five cells that form the stack. Δp was measured at mean linear flow rate within the range of 0.26–12.5 cm s^{-1} for the bromine compartment. Pressure sensors were located in T-pieces in the external manifold of the cell (see Fig. 2) and the data were monitored and stored with a purpose built data acquisition program run from a PC. Fig. 6 shows the logarithmic plot of pressure drop as a function of the logarithm of the mean flow velocity. Δp across the bromine compartment was higher than the pressure drop across commercially available reactor, such as the FM01-LC; this is mainly due to the flow restrictions imposed by the spirals in the manifold which are important in minimizing bypass currents [40,41].

Fig. 6 shows that the pressure drop in the bromine compartment changes logarithmically with the flow velocity. The experimental data can be fitted to the equation: $\Delta p = 0.03v^{1.6}$, for pressure drop values above mean linear flow velocity of 2 cm s^{-1}. The pressure drop can also be related to the mass transport coefficient; ideally, high rates of mass transport and low pressure drop are desirable and a compromise should be achieved between reasonable low pressure drop and transport coefficients. Fig. 7 shows that the mass transport coefficient increases with Δp within the reactor. The pressure drop measured when the mass transport coefficient was evaluated at the nominal mean linear flow rate of 2 cm s^{-1} was approximately 0.1 bar, as it is shown in the figure.

3.3. Flow dispersion

Dispersion experiments were carried out at mean linear flow velocities within the range of 1–10 cm s^{-1} at 298 K. Fig. 8 shows the conductivity of KCl *versus* time at the outlet of the bromine compartment. It can be seen from the figure that at low flow rates (e and f) the curves show a shoulder in the rising left hand side. The shoulder is less prominent as the mean flow rate increases and at the highest flow rates there is practically a single peak flow distribution. This indicates two phase flow dispersion in this compartment, which is revealed clearly at low flow rates.

Fig. 9 shows a plot of the mean linear flow rate *versus* time of appearance of the peaks that represent the slow and fast phases. The shoulder or first peak appears before the mean residence time, calculated from the ratio of reactor volume and volumetric flow rate, while the second peak emerges just after the mean residence time. As the flow rate increases, the time at which the shoulder appears approaches the time of the second peak and

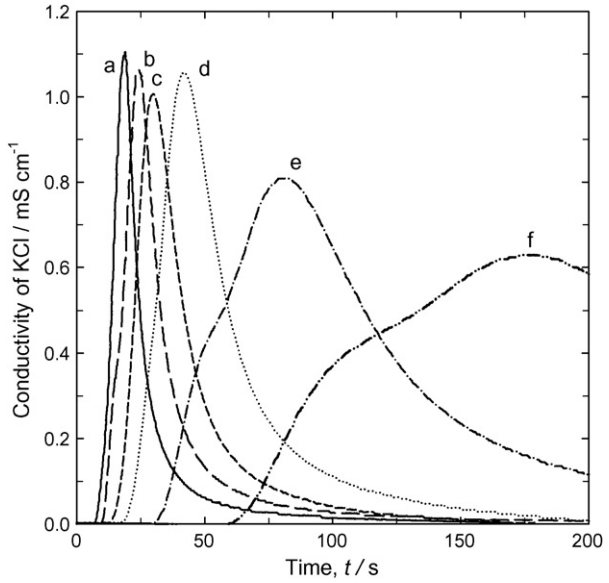

Fig. 8. Dispersion curves of electrolyte conductivity *vs.* time at different flow rates for the bromine compartment. Mean linear electrolyte velocities: (a) 10.4 cm s^{-1}, (b) 7.8 cm s^{-1}, (c) 5.7 cm s^{-1}, (d) 4 cm s^{-1}, (e) 2 cm s^{-1} and (f) 1 cm s^{-1}.

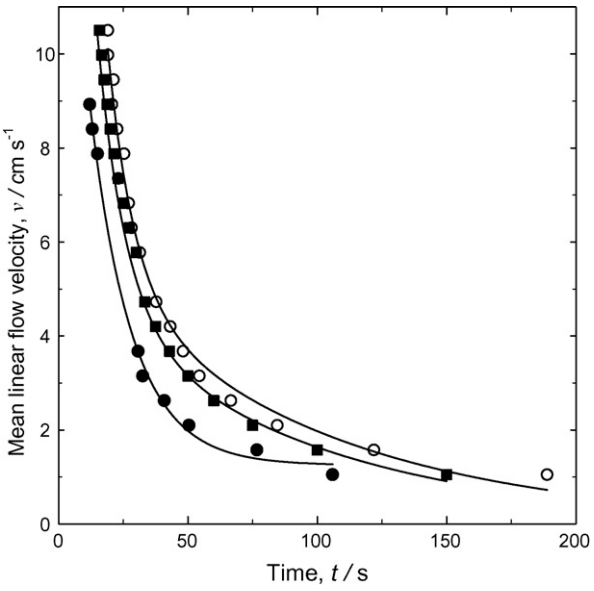

Fig. 9. Mean linear flow velocity *vs.* time for appearance of the first and second peaks from the compartment of the reactor and the theoretical residence time, at various flow rates. (●) First peak in Fig. 8, (◯) second peak in Fig. 8 and (■) calculated residence time in the reactor.

both phases leave the reactor at times close to the calculated residence time.

4. Conclusions

The reaction environment in a five-bipole, electrochemical filter-press reactor used as a redox flow cell stack, has been characterised by mass transport, pressure drop and fluid dispersion measurements.

1. The mass transport characteristics of the reactor were evaluated from dissolved bromine concentration decay curves. The Sherwood *versus* Reynolds correlations were compared with other large scale electrochemical reactors. The present reactor operates at low Reynolds numbers because it was primarily designed for operation under charge transfer controlled reaction conditions.
2. There was an increase of pressure drop across the reactor with the mean flow velocity that can be expressed by the approximate correlation $\Delta p/\text{bar} = 0.03[v/\text{cm s}^{-1}]^{1.6}$.
3. The flow distribution in the reactor has been evaluated using a perturbation–response technique. The dispersion curves suggested the existence of a fast phase which leaves the reactor before the calculated mean residence time and a slow phase that exceed the mean residence time. The two flow phases can be distinguished at mean linear flow velocities below 6 cm s^{-1}. At higher mean linear flow velocities the two phases merged leaving the compartment at times that approach the calculated mean residence time.

Acknowledgements

The authors gratefully acknowledge partial financial support by Regenesys Technologies Ltd. and contributions to early work by D.A. Szánto and many colleagues at Regenesys Technologies Ltd. The authors are also grateful to John Bishop from the Department of Chemical Engineering at the University of Bath for advice and construction of some electronic equipment used in this work. Early parts of this work were performed in the Department of Chemical Engineering at the University of Bath, UK.

Appendix A. Nomenclature

A	geometrical area of the electrode (cm^2)
B	breadth of the electrode (cm)
$c_{(t)}$	concentration of reactant, in the tank, at time t
$c_{(0)}$	concentration of reactant, in the tank, at time zero
d_e	equivalent diameter of flow channel (cm)
D	diffusion coefficient of Br^- ions ($cm^2\ s^{-1}$)
k_m	mass transport coefficient ($cm\ s^{-1}$)
Δp	pressure drop (bar)
Q	volumetric flow rate of electrolyte ($cm^3\ s^{-1}$)
S	separation between the electrode and the membrane (cm)
t	time (s)
v	mean linear flow velocity of electrolyte ($cm\ s^{-1}$)

Greek letters

ν	kinematic viscosity of electrolyte ($cm^2\ s^{-1}$)
τ_R	mean residence time in the reactor (s)
τ_T	mean residence time in the tank (s)

References

[1] D.J. Pickett, Electrochemical Reactor Design, 2nd ed., Elsevier, Amsterdam, 1979.
[2] D. Pletcher, F.C. Walsh, Industrial Electrochemistry, 2nd ed., Chapman & Hall, London, 1990.
[3] F. Goodridge, K. Scott, Electrochemical Process Engineering: A Guide to the Design of Electrolytic Plant, Plenum Press, New York, London, 1995.
[4] F.C. Walsh, D. Robinson, Electrochem. Soc. Interf. 7 (1998) 40.
[5] J.H. Hammond, D. Robinson, F.C. Walsh, in: G. Kreysa (Ed.), Electrochemical Cell Design and Optimisation Procedures, John Wiley & Sons, Inc., Frankfurt Germany, Dechema Monographs 123 (1990) 279.
[6] G. Kreysa (Ed.), Electrochemical Cell Design and Optimisation Procedures, Frankfurt, Germany, Dechema Monographs 123 (1990).
[7] R.J. Marshall, F.C. Walsh, Surf. Tech. 24 (1985) 45.
[8] D. Chai, D. Genders, N. Weinberg, G. Zappi, E. Bernasconi, J. Lee, J. Roletto, L. Sogli, D. Walker, C.R. Martin, V. Menon, P. Zelenay, H. Zhang, Org. Process. Res. Dev. 6 (2002) 178.
[9] M. Kupper, V. Hessel, H. Lowe, W. Stark, J. Kinkel, M. Michel, H. Schmidt-Traub, Electrochim. Acta 48 (2003) 20.
[10] C. Belmont, H.H. Girault, J. Appl. Electrochem. 24 (1994) 719.
[11] C. Pliangos, C. Raptis, I. Bolzonella, Ch. Comninellis, C.G. Vayenas, Ionics 8 (2002) 372.
[12] J.M. Bisang, J. Appl. Electrochem. 23 (1993) 966.
[13] J.-G. Jiang, N. Graham, C. Andre, G.H. Kelsall, N. Brandon, Water Res. 36 (2002) 4064.
[14] U. Ogutveren, T.E. Bakir, S. Koparal, Water Res. 33 (1999) 1851.
[15] N. Mameri, H. Lounici, D. Belhocine, H. Grib, D.L. Piron, Y. Yahiat, Sep. Purif. Tech. 24 (2001) 113.
[16] J.A. Drake, C.J. Radke, J. Newman, Ind. Eng. Chem. Res. 40 (2001) 3117.
[17] K. Scott, W. Hui, J. Appl. Electrochem. 26 (1996) 10.
[18] M.L. Lin, Y.Y. Wang, C.C. Wan, J. Appl. Electrochem. 22 (1992) 1197.

[19] H. Karami, M.F. Mousavi, M. Shamsipur, J. Power Sources 124 (2003) 303.
[20] M. Ruge, F.N. Buchi, Proceedings of the Energy and Electrochemical Processing for a Cleaner Environment, San Francisco, California, September 2–7, Electrochem. Soc. 23 (2001) 165.
[21] M. Ghouse, J. Appl. Electrochem. 28 (1998) 955.
[22] D. Buttin, M. Dupont, M. Straumann, R. Gille, J.-C. Dubois, R. Ornelas, G.P. Fleba, E. Ramunni, V. Antonucci, A.S. Aricoá, P. Cretiá, E. Modica, M. Pham-Thi, J.-P. Ganne, J. Appl. Electrochem. 31 (2001) 275.
[23] S.S.I. Lee, J.M. McIntosh, R.J. Vohs, R. Gorte, Proceedings of the Solid Oxide Fuel Cells Paris, France, April 27–May 2, Electrochem. Soc. 7 (2003) 865.
[24] D.P. Davies, P.L. Adcock, M. Turpin, S.J. Rowen, J. Appl. Electrochem. 30 (2000) 101.
[25] M. Bursell, A. Lundblad, P. Bjoernbom, Proceedings of the Advances in Electrochemical Capacitors and Hybrid Power Systems, Philadelphia, Pennsylvania, May 12–17, Electrochem. Soc. 7 (2002) 116.
[26] N.D. Ivanova, A.I. Gerasimchuk, N.E. Vlasenko, Russ. J. Appl. Chem. 75 (2002) 1079.
[27] A. Price, S. Bartley, S. Male, G. Cooley, Power Eng. J. 13 (1999) 122.
[28] C. Ponce de León, A. Frías-Ferrer, J. González-García, D.A. Szánto, F.C. Walsh, J. Power Sources 160 (2006) 716.
[29] F.C. Walsh, Pure Appl. Chem. 73 (2001) 1819.
[30] Ch.M. Hagg, M. Skyllas-Kazacos, J. Appl. Electrochem. 32 (2002) 1063.
[31] T. Sukkar, M. Skyllas-Kazacos, J. Appl. Electrochem. 34 (2004) 137.
[32] M. Gattrell, J. Park, B. MacDougall, J. Apte, S. McCarthy, C.W. Wu, J. Electrochem. Soc. 151 (2004) A123.
[33] M. Bartolozzi, J. Power Sources 27 (1989) 219.
[34] A.T.S. Walker, A.A. Wragg, Electrochim. Acta 22 (1977) 1129.
[35] Regenesys utility scale energy storage: project summary. Dti reports available online at: http://www.ecdti.co.uk/cgibin/perlcon.pl [Accessed February 23, 2007].
[36] T.J. Calver, S.E. Male, P.J. Mitchell, I. Whyte, Carbon Based Electrodes, International Application Number: PCT/GB99/01396; International Patent Classification: H01M 4/96, 8/18; International Publication Number: WO 99/57775.
[37] D.G. Clark, J.S. Hampden, H.S. Oates, The Electrochemical Cell, International Application Number: PCT/GB99/03158; International Patent Classification: H01M 8/02, 8/24, C25B 15/08; International Publication Number: WO 00/19554.
[38] F.C. Walsh, A First Course in Electrochemical Engineering, The Electrochemical Consultancy, Romsey, 1993.
[39] W.P.J. Ford, F.C. Walsh, I. Whyte, I. Chem. E. Symp. Ser. 127 (1992) 111.
[40] R.A. Scannell, F.C. Walsh, I. Chem. E. Symp. Ser. 112 (1989) 59.
[41] K. Scott, W. Taama, B.R. Williams, J. Appl. Electrochem. 28 (1998) 259.
[42] D.R. Lide (Ed.), Handbook of Chemistry and Physics, 87th ed., CRC Taylor & Francis, New York, 2006–2007.
[43] I. Vogel, A. Mobius, Electrochim. Acta 36 (1991) 1403.